

Ab initio description of magnetic and critical properties of spin-glass pyrochlore $\text{NaSrMn}_2\text{F}_7$

Mohammad Amirabbasi*

*Department of Physics, Isfahan University of Technology (IUT), Isfahan 84156-83111, Iran
Faculty of Physics, University Duisburg-Essen, 47057 Duisburg, Germany and*

Corresponding author email: mo.amirabbasi@gmail.com

(Dated: May 9, 2023)

In this study, I have investigated the magnetic and critical properties of manganese pyrochlore fluoride $\text{NaSrMn}_2\text{F}_7$, which exhibits a glass transition at $T_f=2.5$ (K) due to charge disorder. A DFT+ U +SOC framework is used in this paper to derive spin-Hamiltonian terms, including isotropic and anisotropic exchange interactions. An optimized geometry reveals a local distortion of the F-Mn-F angle along the $\langle 111 \rangle$ direction (95.48° and 84.51°), which is considered a weak bond disorder (δJ). In spite of the complex structure of this material, first principle calculations show that its magnetic properties are only controlled by the nearest neighbor's Heisenberg exchange interaction, and other interactions do not affect spin arrangements in the ground state. Thus, this material is considered a suitable candidate for studying electron correlation in spin glasses. Using a replica-exchange framework, Monte Carlo simulations indicate that with $\delta J=0$, no phase transition is observed when magnetic susceptibility changes with temperature. Based on δJ and the spin Hamiltonian, 2.6 (K) is obtained as the phase transition temperature.

PACS numbers: 71.15.Mb, 75.40.Mg, 75.10.Hk, 75.30.Gw

I. INTRODUCTION

Spin-glass (SG) is a type of magnetic phase in which the spatial arrangement of spins at low-temperatures is completely random¹⁻⁴. The presence of frustration (co-existing and competing ferromagnetic and antiferromagnetic interactions) and randomness (such as chemical disorders or weak bond disorders) are essential for glass formation^{1,2,6}. These materials undergo a second-order phase transition which makes the study of SG materials attractive to scientists⁶. Experimental evidence to detect such a phase are bifurcation of the field cooled (FC) and zero field cooled (ZFC) of DC susceptibility, frequency dependence of AC susceptibility, no magnetic saturation even at low-temperature and high magnetic field and diffusive peaks inelastic neutron scattering pattern^{1,3,7}. In recent years, some geometrically frustrated pyrochlores have shown the SG phase^{8,9}. These materials are composed of a network of corner-sharing tetrahedra^{10,11}. If the exchange interaction between the nearest neighbor is antiferromagnetic, the system fails to reach the ground state with a global minimum. This condition is called geometric frustration¹⁰⁻¹³. Despite many studies and researches, there are still many questions about what is the truly thermodynamic SG transition². Determination of the ground state of classical Heisenberg antiferromagnetic SG pyrochlores in which only Heisenberg interactions play a key role can be a good candidate to answer these questions.

In 1997, with the discovery of the spin-ice phase in $\text{Ho}_2\text{Ti}_2\text{O}_7$ ¹⁴, study on the magnetic properties of oxide pyrochlores increased¹⁵⁻²¹. One of the main problems in the study of these materials is the difficult conditions of their crystal growth. As a consequence, the availability of large crystal pyrochlores in large sizes has

made it impossible. There is no such problem for pyrochlore fluoride with general chemical formula $\text{A}_2\text{B}_2\text{F}_7$ in which $\text{Na}^{1+}/\text{Sr}^{2+}(\text{Ca}^{2+})$ atoms occupy A-site position randomly and magnetic atoms such as Mn^{2+} , Fe^{2+} , Co^{2+} and Ni^{2+} occupy B-site^{5,22-24}. The result of this random occupation is the presence of the δJ (difference in the bond angle between the magnetic ions). Therefore, all of these materials exhibit SG properties at low-temperatures^{9,25}. In this paper, I intend to investigate the magnetic and critical properties of $\text{NaSrMn}_2\text{F}_7$ which has the largest spin moment among the pyrochlore fluoride by first-principle methods in the framework of DFT and Monte Carlo (MC) simulation. In this material, the Mn^{2+} terminates in $3d^5$. Therefore, $S=5/2$ and the orbital moment has a small contribution to the effective moment ($6.25 \mu_B/\text{Mn}^5$). The absence of orbital moment and its associated complexities make this material a suitable candidate to study the effect of bond weak disorder in the phase transition of SG ground state.

The lattice of the $\text{NaSrMn}_2\text{F}_7$ consists of two separate sublattices with corner-shared tetrahedra (Fig. 1). In one sublattice, the $\text{Na}^{1+}/\text{Sr}^{2+}$ ions and in the other the magnetic ion (Mn^{2+}) sit on the vertices of each tetrahedra. The space group of this pyrochlore is Fd-3m (No. 227). Accordingly, the $\text{Na}^{1+}/\text{Sr}^{2+}$, Mn^{2+} and F^{1-} occupy the 16d (0.5, 0.5, 0.5), the 16c (0, 0, 0), 48f (x , 1/8, 1/8) and the 8b (3/8, 3/8, 3/8), respectively. The only variable parameter in this structure is the x -positional parameter. This parameter ($x=0.3331^5$) controls the bond angle (Mn-F-Mn) and bond length (Mn-F) which plays a decisive role in the magnetic properties. Experimental measurements show that this material is an insulator and shows a SG transition at 2.5 (K)⁵. The most important reason for SG transition can be attributed to the change in the bond angle due to the presence of charge

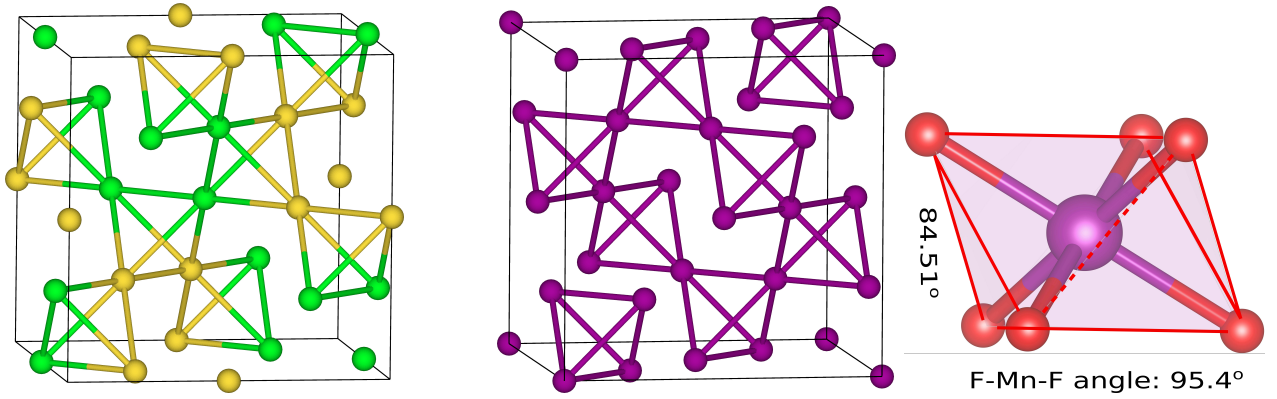


FIG. 1: (Color online) Crystal structure of SG pyrochlore $\text{NaSrMn}_2\text{F}_7$ with corner-shared tetrahedrons for (Left) A-site (Na-Sr atoms) and (right) B-site (Mn atoms). Green, yellow and purple spheres are Na^{1+} , Sr^{2+} and Mn^{2+} , respectively. $x=0.3331$ is experimental value which is reported from the X-ray measurement⁵. The experimental F-Mn-F bond angles in $\langle 111 \rangle$ direction, lattice constant and F-Mn bond length in this material are 80.9 and 99.1° , 2.06 Å and $10.8012(3)$ Å, respectively⁵.

disorder ($\text{Na}^{1+}/\text{Sr}^{2+}$) in the lattice⁵. The interaction between Mn^{2+} ions is the superexchange mediated by F^{1-} . This mechanism is directly related to the bond length and bond angle. Around each Mn ions, there is a flattened octahedra by F ions. In this octahedra, the F-Mn-F angles are different in $\langle 111 \rangle$ direction (97.8° and 82.2°)⁵. The change in F-Mn-F bond angle causes variations in exchange parameters. As a result, the ground state of the system takes SG order. The Curie-Weiss temperature (θ_{CW}) equals -89.72 (K) which indicates the presence of strong antiferromagnetic interactions between magnetic ions⁵.

Microscopic examination of the exchange interactions in this material and its effect on the formation of the SG phase as well as the study of the critical properties seem interesting. This paper aims to determine magnetic and critical properties of $\text{NaSrMn}_2\text{F}_7$ by constructing a spin Hamiltonian model. It includes various interactions such as the Heisenberg exchange parameters up to the third neighbor, the bi-quadratic, single-ion anisotropy (SIA) and Dzyaloshinskii-Moriya interactions (DMI) as obtained by the first-principle methods. By using this information, one can obtain the critical properties of this material, including transition temperature. The current calculations show that only the $J_1 + \delta J$ is important in determining the magnetic properties of this material, and the effect of other interactions is negligible. As a result, this material is considered as a simple model of SG and it can be a good candidate for further studies such as understanding the electron-electron correlation influence on magnetic ground state²⁶ especially in the SG phase, the effect of δJ on thermal fluctuations and removing huge degeneracy²⁵ and what is the border between SG and liquid phase according to the strength of δJ ²⁷⁻²⁹.

The paper is structured as follows. In section II the details of the DFT and MC computational methods have been presented. Section III is devoted to deriving the spin Hamiltonian and the different aspects of exchange interactions in determination of magnetic ground state of

$\text{NaSrMn}_2\text{F}_7$ and in the following, the critical properties are discussed. Finally, In section IV a summary is given.

II. COMPUTATIONAL METHODS

In this paper, I introduce the classical spin Hamiltonian (H) to get magnetic properties of SG pyrochlore $\text{NaSrMn}_2\text{F}_7$:

$$H_{\text{spin}} = -\frac{1}{2} \sum_{i \neq j} J_{ij} (\vec{S}_i \cdot \vec{S}_j) + \frac{1}{2} B \sum_{\text{n.n}} (\vec{S}_i \cdot \vec{S}_j)^2 + \frac{1}{2} D \sum_{\text{n.n}} \hat{D}_{ij} \cdot (\vec{S}_i \times \vec{S}_j) + \frac{1}{2} \Delta \sum_i (\vec{S}_i \cdot \vec{d}_i)^2 \quad (1)$$

where \vec{S}_i denotes magnetic spins, vector \hat{D}_{ij} shows direction of DM which is determined by Moriya's rules^{30,31} and vector \vec{d}_i is the single-ion easy-axis direction at each site i . According to Moriya's rules, if the mirror planes join two sites and the middle point of the opposite bond then the DM vectors should be perpendicular to the mirror plane^{30,31}. It should be noted that in this model $|\vec{S}|=1$. Different terms of spin Hamiltonian express different types of exchange interactions without (isotropic terms) and with (anisotropic terms) considering spin-orbit coupling (SOC). Isotropic terms, J_{ij} and B are Heisenberg and bi-quadratic coupling, respectively. Heisenberg interaction decreases rapidly with distance because the $\text{NaSrMn}_2\text{F}_7$ is an insulator. Therefore, Heisenberg terms are calculated up to the third nearest neighbor (J_1 , J_2 and J_{3a}). To this end, one has to regard the conventional unit-cell (88 atoms) with $4 \times 4 \times 4$ optimized Monkhorst-Pack k-point mesh. Then, J_1 , J_2 and J_{3a} values can be obtained by calculating the total energy of different collinear spin configurations and mapping them to the Heisenberg model (Fig. 2 and Fig. 6). There are two possible third nearest neighbor exchange

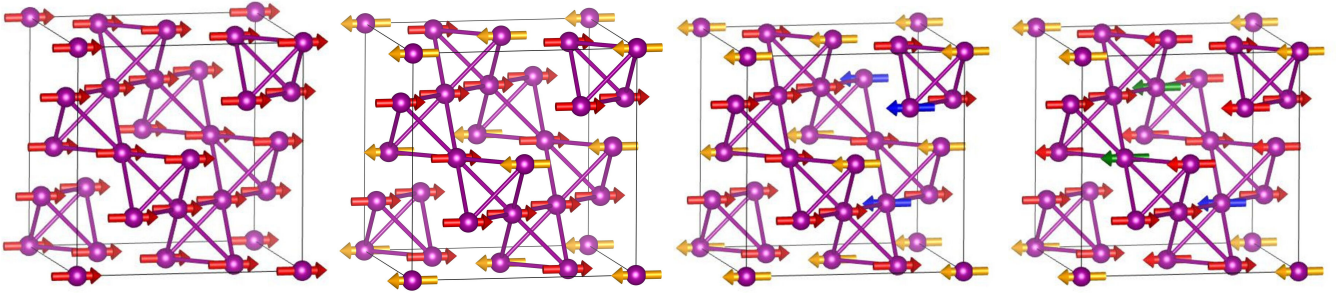


FIG. 2: (Color online) Different collinear spin configurations for calculation Heisenberg couplings. The purple spheres denote Mn^{2+} . The arrows indicate the direction of the spins for each atom. From left to right, the colors of some of the spins are selected differently to distinguish between different configurations. The ferromagnetic configuration has been chosen as the reference to calculate the total energy difference of the various configurations. In this paper, 20 different spin configurations have been used to make sure that the J_1 converges with respect to the number of configurations.

interaction in this structure, J_{3a} and J_{3b} ^{32–34}. Generally, in the cubic pyrochlore structures $J_{3b} \ll J_{3a}$. Therefore, J_{3b} is approximated 0^{32–34}.

The nearest neighbor coupling is important for B and anisotropic terms such as Dzyaloshinskii-Moriya coupling (D) and single-ion anisotropy strength (Δ). Therefore, the primitive cell (22 atoms) with $6 \times 6 \times 6$ optimized Monkhorst-Pack k-point mesh must be regarded. The strength of B can be determined via total energy of non-collinear spin configurations in the absence of spin-orbit coupling (GGA+ U). In this case, if one starts from the all-in/all-out spin configuration (where all spins are oriented towards in/out center of tetrahedra) and if one rotates the spins so that $\vec{S}_1 + \vec{S}_2 + \vec{S}_3 + \vec{S}_4 = 0$, it can be shown that Heisenberg term is degenerated³⁴. The total energy difference of different noncollinear spin configurations can be attributed to B ³⁴.

With the uniform rotation of magnetic moments in the absence of SOC, the isotropic terms of the spin Hamiltonian are degenerated. By considering the spin-orbit coupling (GGA+ U +SOC), the total energy difference of the various noncollinear spin configurations is entirely attributed to D provided that the SIA is negligible³⁴. Given that Mn^{+2} ends in $3d^5$, it is expected that SIA has a very small contribution. To calculate this term, one has to examine two different noncollinear spin configurations. In the first spin configuration, one magnetic moment points outward from the center of the tetrahedra. The other three moments point inward toward the center of the tetrahedra. For the second spin configuration, the magnetic moments of the first configuration rotate about 120° around the Z axis. It can be demonstrated that for these two spin configurations in the absence of SOC, isotropic terms do not change. In the presence of SOC, the D remains unchanged and the total energy difference between these two spin configurations is entirely attributed to Δ ³⁵.

The derivation Heisenberg term and Other terms of Eq. (1) have been done by the full-potential linearized augmented plane wave (FPLAW) method as implemented in the FLEUR³⁶ code and Quantum Espresso

(QE)^{37,38} code which employs the plane wave basis set, respectively. For the exchange-correlation energy, I employ the Perdew Burke Ernzerhof parametrization of the generalized gradient approximation (GGA)³⁹. The GGA+ U approximation⁴⁰ is used to account for the on-site Coulomb interaction for $3d$ orbitals of Mn atoms. The optimized cut-off of wave function expansion in the interstitial region is set to $k_{\text{max}} = 4.2 \text{ a.u.}^{-1}$. The muffin-tin radius of Na, Sr, Mn and F atoms are set to 2.6, 2.8, 2.3 and 1.4 a.u., respectively. To increase the accuracy of the calculations, I have considered the 3s and 3p orbitals of the Mn as semicore electrons (FLAPW+LO). The effective U parameter ($U_{\text{eff}} = U - J_{\text{H}}$), where U and J_{H} are screened on-site Coulomb and Hund exchange interactions, is calculated by the Density Functional Perturbation Theory (DFPT)⁴¹ using the QE code. The optimized 40 Ry and 400 Ry cutoff have been considered for expanding wavefunction and charge density in plane wave, respectively. The approximation electron-ion interaction has been controlled through GBRV ultra-soft pseudo-potential⁴². In order to investigate the effect of random distribution on A-site, one considers a conventional unitcell with 88 atoms. For this unitcell, 97 different configurations with different A-site distributions can be defined by using the supercell program⁴³. Each of these distributions has a specific and unique symmetry. For calculations of the total energy for each configuration, QE code has been used in GGA approach.

To capture the critical properties and low-temperature spacial spin arrangement of $\text{NaSrMn}_2\text{F}_7$, one performs MC simulation. The effect of charge disorder has been regarded in this simulation. Since SG materials have multiple local minimums in their energy landscape, reaching to a global minimum specially at low-temperature is not possible. To tackle this problem, the replica exchange method⁴⁴ should be employed as implemented in the ES-pinS package⁴⁵. The Gaussian distribution has been considered as the particular choice of disorder. In the replica exchange algorithm, the high-temperature configurations are swapped for the low-temperature configurations so that the system reaches thermal equilibrium. The con-

TABLE I: For various U_{eff} values, Heisenberg couplings up to third neighbors have been determined. A negative value denotes anti-ferromagnetic exchange interaction, whereas a positive value denotes ferromagnetic exchange interaction. T_f can also be determined via MC simulations. To account for the effect of random A-site occupations, $\delta J=0.13(\text{meV})$ can be regarded as a weak bond disorder.

U_{eff} (eV)	J_1 (meV)	J_2 (meV)	J_3 (meV)	T_f (K)
4.58	-1.97	-0.03	0.02	1.8
4.00	-2.33	-0.04	0.03	2.6
EXP				2.5 ⁵

dition for the system to reach equilibrium is that the MC steps should be sufficiently selected so that, first, the temperature behavior of the specific heat and energy of the system is smooth and, second, the position of the specific heat peak changes slightly by changing the seed and third, the acceptance ratio of MC steps at each temperature reaches at least to 65 percent. The linear size of the simulation cell ($L=16$) is used to ensure the presence of phase transition. In this way, there are $N \times L^3$ spins in the three-dimensional lattice where N is the number of spins ($N=4$ for one tetrahedron). For MC calculations,

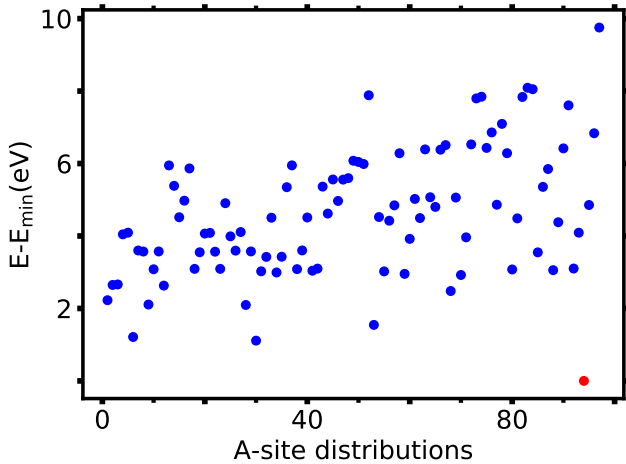


FIG. 3: (Color online) *Ab initio* calculations of total energy for different A-site distributions in GGA approach. The red circle which has minimum total energy is related to homogeneous distribution in which Na and Sr occupy A-site tetrahedral with two by two ratio. The total energy of homogeneous distribution has been considered as E_{min} . It should be noted that primitive cell for calculating exchange parameters beyond Heisenberg term can be made only for the homogeneous distribution.

when δJ is considered, the calculations are performed for ten different starting points (different seeds) and then the final result is expressed as the average of them. 3×10^6 MC steps per spin at each temperature are performed for the thermal equilibrium and data collection, respectively. To reduce the correlation between the successive data, measurements are done after skipping every 10 MC steps.

III. RESULTS AND DISCUSSION

A. Different distributions of Na-Sr on A-site

A-site is completely randomly occupied by Na/Sr with equal concentrations. I take into account 97 various configurations with various A-site distributions with a distinct and special symmetry in order to examine the impact of varied A-site distributions on structural and magnetic properties. First, I compute the total energy of all 97 distributions. The diagram reffig:tf depicts how the different 97 configurations are arranged in terms of total energy. In the GGA approach, I use the QE code for this calculation. One distribution has the lowest total energy, according to Fig. 3. I call it homogeneous distribution because Na-Sr occupy A-site in such a way that there are two Sr and two Na in each A-site tetrahedral. For this distribution, one can only make primitive cells with 22 atoms. Although the obtained band structure (Fig. 4) suggests that the material is an insulator in the GGA approach, one needs to describe accurately the electron-electron Coulomb correlation due to the 3d orbital of the Mn atom. Therefore, one should apply the Hubbard potential to 3d electrons as an on-site Coulomb interaction. Based on the *ab initio* calculations (DFPT method), the effective Hubbard parameter U_{eff} obtains 4.58 eV for this system. In this paper, I have taken into account $J_H \sim 1.0$ eV as it is suggested for 3d materials^{46,47}. After determining the U parameter, I optimize the primitive cell's lattice constants and ion locations. To eliminate bias, I examine FM order and maintain symmetry so that the final geometry has the same experimental symmetry and space group as the original geometry. The obtained results reveal that the F-Mn-F angle is distorted in the $\langle 111 \rangle$ direction (see Fig. 1). The estimated values are 95.48° and 84.51° , which accord well with the experimental values (97.8° and 85.2°). The optimized x parameter and lattice constant are 0.3337 and 10.8930Å, respectively, which are equivalent to the experimental values 0.3331 and 10.8012Å.

B. Magnetic and electronic properties

The quantitative derivation spin Hamiltonian (Eq. (1)) is effective to explain or predict the magnetic proper-

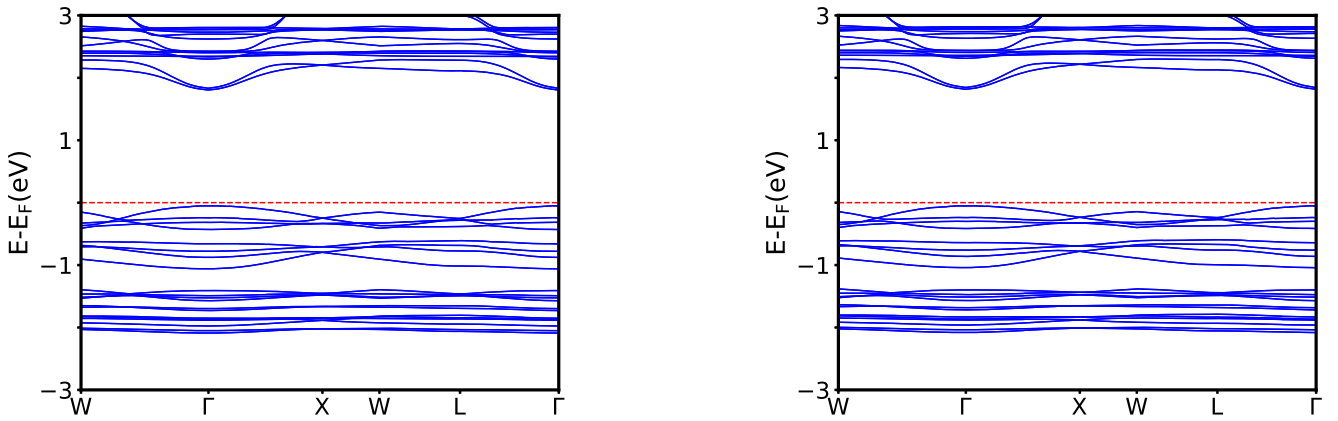


FIG. 4: (Color online) Obtained the band structure of NaSrMn₂F₇ in **(Left)** GGA and **(Right)** GGA+SOC approaches, respectively. The Fermi energy is set to zero. The all-in/all-out magnetic configuration (noncollinear spin texture) has been considered for these calculations. The figures exhibit that the SOC has an ignorable effect on energy bands near the Fermi level.

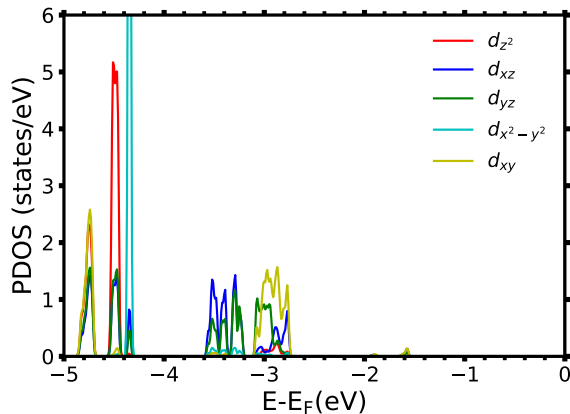


FIG. 5: (Color online) PDOS calculated for AFM-ordered NaSrMn₂F₇ using the GGA functional. It illustrates the local 3d DOS of a single Mn atom for majority spins. The obtained Lowdin Charge analysis indicates that the majority spin levels are fully occupied and minority spin levels are negligibly occupied. That's why the 3d DOS for minority of spins has not been exhibited. It should be noted that this calculation has been done by using QE code^{37,38}.

ties of this pyrochlore. This information can answer the fundamental question about how a novel ground state emerges. The results of calculations of different spin Hamiltonian terms for different Hubbard parameters are given in Table. I. To ensure the exact value of U_{eff} , T_f obtained from the MC simulation can be compared with the experimental value. As shown in Table. I, I have started from $U_{\text{eff}}=4.58$ eV and decreased it until the obtained T_f is equal to the experimental value. In this way, the optimum U_{eff} is 4.0 eV.

According to the chemical valence of different atoms in NaSrMn₂F₇ compound, one expects that Na, Sr, Mn and F are in the +1, +2, +2 and -1 oxidation states, respec-

tively. Therefore, the external shell of Mn⁺² is 3d⁵ and Hund rule predicts a spin $S=5/2$, and thereby a magnetic moment $5 \mu_B$ for it. The DFT calculations obtain $4.8 \mu_B$, not far from the native ionic picture. With this simple picture, one expects the quantum angular momentum of Mn to be zero and the magnetization of this compound originated only from spin part. The DFT calculations give some residual magnetization $0.024 \mu_B$, $0.0008 \mu_B$ and $0.0005 \mu_B$ for F, Sr and Na atoms, respectively.

To ensure that the bond disorder does not affect the crystal field and its consequences for higher order exchange interactions, other important and effective exchange couplings must be calculated. DFT calculations show that other exchange parameters like B , D , and Δ are 3 to 4 times smaller than J_1 . As a result, these interactions are negligible and have no bearing on the magnetic properties of the ground state. The orbital moment of the magnetic ion strongly influences the antisymmetric exchange interactions (DMI and SIA). The Mn orbital moment plays a very small role in the effective orbital of this material, according to experimental measurements⁵. The orbital moment of each Mn ion obtained from *ab initio* calculations (GGA+ U +SOC) is $0.0001 \mu_B$, which is a very small amount. It is possible to conclude that antisymmetric exchange interactions in this material are unimportant. Fig. 4 also compares band structures for noncollinear (all-in/all-out) magnetic configurations with and without SOC. As can be seen, the SOC has very little effect on the energy bands, especially near the Fermi level. As a result, the SOC effect in this material is very weak. The spin-projected DOS (PDOS) and Lowdin charge analysis calculations for a Mn atom confirm that the SOC effect is negligible (Fig. 5). According to the Lowdin charge analysis, the total charge for majority and minority spin levels are $d_{z^2}=0.9973$, $d_{xz}=0.9905$, $d_{yz}=0.9909$, $d_{x^2-y^2}=0.9973$, $d_{xy}=0.9927$ and $d_{z^2}=0.0348$, $d_{xz}=0.0723$, $d_{yz}=0.0707$,

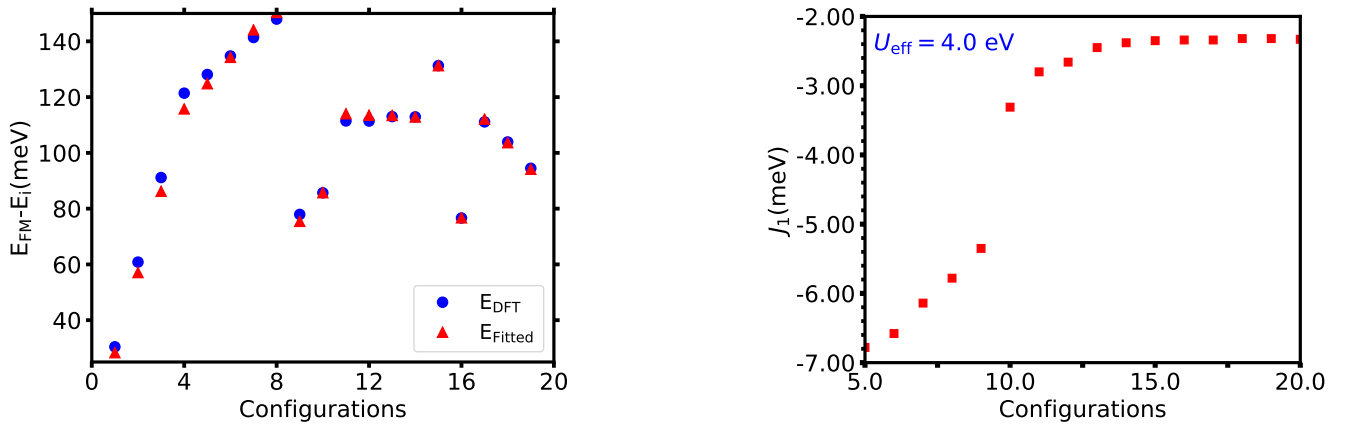


FIG. 6: (Color online) (**Left**) Mapping total energy for various collinear spin configurations obtained by DFT+ U into the Heisenberg model. The error of fitting is 2%. (**right**) Variation of J_1 with respect to different random collinear spin configurations. After 20 different configurations, J_1 trend has been constant.

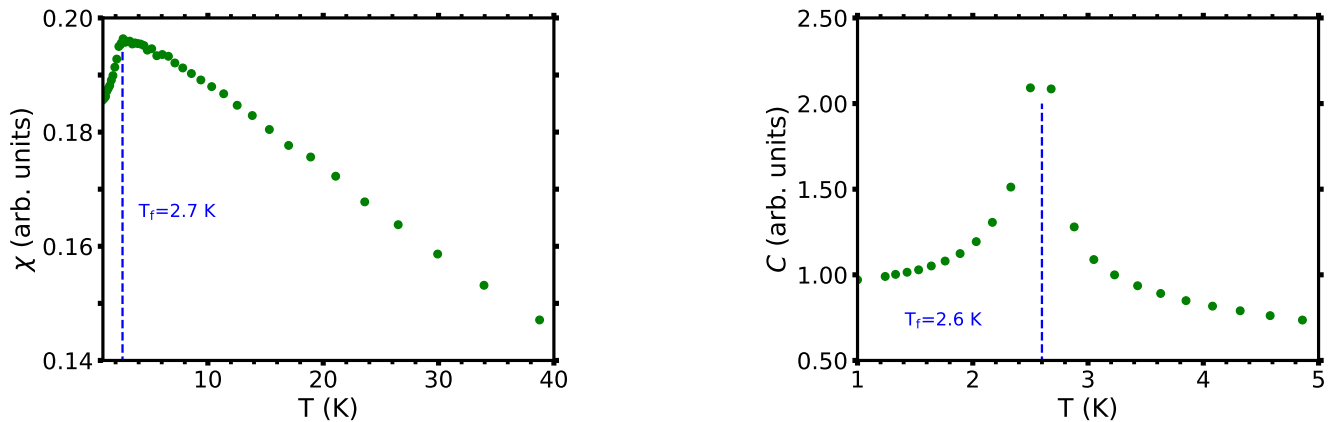


FIG. 7: (Color online) The calculated (**Left**) magnetic specific heat and (**right**) magnetic susceptibility for $\delta J=0.13$ (meV). The obtained freezing temperature is similar to the experimental value. The temperature of the peak has been considered as T_f because this point is where the break between high and low temperature data is defined. $L=16$ has been used as the size of the simulation lattice for these calculations.

$d_{x^2-y^2}=0.0358$, $d_{xy}=0.0723$, respectively. As a result, the majority spin levels are completely occupied, while the minority spin levels are barely occupied. It is reasonable to conclude that the orbital moment is quenched in this material. Fig. 6 shows how J_1 has been calculated. As one can see, the choosing number of different collinear magnetic configurations continues until J_1 reaches a constant value which is -2.33 (meV). Also, Fig. 6 illustrates how the total energies from DFT+ U calculations are mapped to the Heisenberg model via the least-square fitting method. The error of fitting obtains 2%. The exchange parameters of the second (J_2) and third (J_3) nearest neighbors are very small. Thus, A-site random occupation only changes J_1 . One can estimate this weak bond disorder by using $\delta J = \sqrt{\frac{3}{8}} k_B T_f$ ⁴⁸. Since the experimental value of the freezing temperature is 2.5 (K)⁵, δJ is equal to 0.13 (meV).

C. Critical properties

In the following, I perform MC simulations to find the optimal U_{eff} and the *ab initio* freezing temperature. The calculations are done taking into consideration δJ to account for the impact of A-site random occupancy on MC simulation. The temperature behavior of the sample's specific heat (C) and magnetic susceptibility (χ) are shown in Fig. 7. I consider the position of peak for C and χ to define freezing temperature. For $\delta J=0.13$ (meV), T_f obtains 2.6 ± 0.1 K. By decreasing the amount of δJ , the freezing temperature decreases so that for $\delta J=0$, no phase transition is observed up to 0.5 K. Therefore, one can conclude that the δJ acts as a small perturbation and must account for the system SG phase transition at low-temperature by eliminating the degeneracy of the ground state⁴⁸.

IV. CONCLUSION

In conclusion, spin Hamiltonian for spin-glass pyrochlore $\text{NaSrMn}_2\text{F}_7$ were calculated using DFT+ U +SOC. The spin Hamiltonian comprised isotropic and anisotropic concepts such nearest neighbor bi-quadratic, Dzyaloshinskii-Moriya, and single-ion anisotropy, as well as Heisenberg coupling up to third neighbors. Since the Hubbard parameter played a decisive role in describing the electron-electron correlation and consequently the magnetic properties, this value was determined via the DFPT method. Then, I reduced it to such an extent that the T_f obtained from the MC simulations equaled to the experimental T_f . The DFT computations revealed that the sole thing that matters most in determining this material's magnetic characteristics is J_1 (as nearest neighbor Heisenberg exchange). Following that, the specific heat and magnetic susceptibility temperature behavior were calculated using the obtained spin Hamiltonian from

MC simulations. Because Na-Sr random occupancy on A-site causes weak bond disorder (δJ), $\delta J=0.13$ (meV) was assumed to produce freezing temperature equals the experimental freezing temperature. δJ behaves like a perturbation and is what causes the spin-glass phase transition at low temperatures because no phase transition can be seen even at low temperatures when $\delta J=0$. To better comprehend the nature of fluctuations at low temperatures and their impact on electron-electron correlation, experimental data like inelastic neutron scattering may be useful.

Acknowledgments

Jülich Supercomputing Centre (JSC) is gratefully acknowledged by author as the provider of needed computing facilities. The guidelines provided by Peter Kratzer, Marjana Ležaić and Mojaba Alaei are highly valued and appreciated.

* Electronic address: mo.amirabbasi@gmail.com

- ¹ J. A. Mydosh, *Spin glasses: an experimental introduction* (CRC Press, 1993).
- ² K. Binder and A. P. Young, *Rev. Mod. Phys.* **58**, 801 (1986).
- ³ T. Taniguchi, T. Munenaka, and H. Sato, in *Journal of Physics: Conference Series*, Vol. 145 (IOP Publishing, 2009) p. 012017.
- ⁴ H. Shintani and H. Tanaka, *Nature Physics* **2**, 200 (2006).
- ⁵ M. Sanders, J. Krizan, K. Plumb, T. McQueen, and R. Cava, *Journal of Physics: Condensed Matter* **29**, 045801 (2016).
- ⁶ H. Kawamura and T. Taniguchi, *Chapter 1 - Spin Glasses*, edited by K. Buschow, *Handbook of Magnetic Materials*, Vol. 24 (Elsevier, 2015) pp. 1 – 137.
- ⁷ E. Vincent and V. Dupuis, in *Frustrated Materials and Ferromagnetic Glasses* (Springer, 2018) pp. 31–56.
- ⁸ K. Mitsumoto, C. Hotta, and H. Yoshino, *Phys. Rev. Lett.* **124**, 087201 (2020).
- ⁹ H. Shinaoka, Y. Tomita, and Y. Motome, *Phys. Rev. Lett.* **107**, 047204 (2011).
- ¹⁰ M. Subramanian, G. Aravamudan, and G. Subba Rao, *Progress in Solid State Chemistry* **15**, 55 (1983).
- ¹¹ J. S. Gardner, M. J. P. Gingras, and J. E. Greedan, *Rev. Mod. Phys.* **82**, 53 (2010).
- ¹² C. Lacroix, P. Mendels, and F. Mila, *Introduction to frustrated magnetism: materials, experiments, theory*, Vol. 164 (Springer Science & Business Media, 2011).
- ¹³ D. Reig-i Plessis and A. M. Hallas, *Phys. Rev. Materials* **5**, 030301 (2021).
- ¹⁴ M. J. Harris, S. T. Bramwell, D. F. McMorrow, T. Zeiske, and K. W. Godfrey, *Phys. Rev. Lett.* **79**, 2554 (1997).
- ¹⁵ D. Slobinsky, L. Pili, G. Baglietto, S. Grigera, and R. Borzi, *Communications Physics* **4**, 1 (2021).
- ¹⁶ R. Moessner and S. L. Sondhi, *Physical Review B* **68**, 064411 (2003).
- ¹⁷ F. P. Marlton, Z. Zhang, Y. Zhang, T. E. Proffen, C. D. Ling, and B. J. Kennedy, *Chemistry of Materials* (2021), 10.1021/acs.chemmater.0c04515.
- ¹⁸ D. Yahne, D. Pereira, L. Jaubert, L. Sanjeeva, M. Powell, J. Kolis, G. Xu, M. Enjalran, M. Gingras, and K. Ross, arXiv preprint arXiv:2101.08361 (2021).
- ¹⁹ Y. Shi, C. Nisoli, and G.-W. Chern, *Applied Physics Letters* **118**, 122407 (2021).
- ²⁰ T. Fennell, P. Deen, A. Wildes, K. Schmalzl, D. Prabhakaran, A. Boothroyd, R. Aldus, D. McMorrow, and S. Bramwell, *Science* **326**, 415 (2009).
- ²¹ S. T. Bramwell and M. J. Gingras, *Science* **294**, 1495 (2001).
- ²² J. W. Krizan and R. J. Cava, *Phys. Rev. B* **89**, 214401 (2014).
- ²³ J. W. Krizan and R. J. Cava, *Phys. Rev. B* **92**, 014406 (2015).
- ²⁴ J. Krizan and R. J. Cava, *Journal of Physics: Condensed Matter* **27**, 296002 (2015).
- ²⁵ A. Andreanov, J. T. Chalker, T. E. Saunders, and D. Sherrington, *Phys. Rev. B* **81**, 014406 (2010).
- ²⁶ A. Alexandradinata, N. Armitage, A. Baydin, W. Bi, Y. Cao, H. J. Changlani, E. Chertkov, E. H. Neto, L. Delacretaz, I. E. Baggari, *et al.*, arXiv preprint arXiv:2010.00584 (2020).
- ²⁷ R. Moessner and J. T. Chalker, *Phys. Rev. Lett.* **80**, 2929 (1998).
- ²⁸ J. Yang, A. Samarakoon, S. Dissanayake, H. Ueda, I. Klich, K. Iida, D. Pajeroski, N. P. Butch, Q. Huang, J. R. Copley, *et al.*, *Proceedings of the National Academy of Sciences* **112**, 11519 (2015).
- ²⁹ O. Cepas and B. Canals, *Physical Review B* **86**, 024434 (2012).
- ³⁰ T. Moriya, *Phys. Rev.* **120**, 91 (1960).
- ³¹ M. Elhajal, B. Canals, R. Sunyer, and C. Lacroix, *Phys. Rev. B* **71**, 094420 (2005).
- ³² B. J. Kennedy, *Physica B: Condensed Matter* **241-243**, 303 (1997), proceedings of the International Conference

- on Neutron Scattering.
- ³³ A. S. Wills, M. E. Zhitomirsky, B. Canals, J. P. Sanchez, P. Bonville, P. D. de Réotier, and A. Yaouanc, *Journal of Physics: Condensed Matter* **18**, L37 (2006).
- ³⁴ A. Sadeghi, M. Alaei, F. Shahbazi, and M. J. P. Gingras, *Phys. Rev. B* **91**, 140407 (2015).
- ³⁵ H. J. Xiang, E. J. Kan, M.-H. Whangbo, C. Lee, S.-H. Wei, and X. G. Gong, *Phys. Rev. B* **83**, 174402 (2011).
- ³⁶ FLEURgroup, "<http://www.flapw.de/>," .
- ³⁷ P. Giannozzi, S. Baroni, N. Bonini, M. Calandra, R. Car, C. Cavazzoni, D. Ceresoli, G. L. Chiarotti, M. Cococcioni, I. Dabo, A. D. Corso, S. de Gironcoli, S. Fabris, G. Fratesi, R. Gebauer, U. Gerstmann, C. Gougoussis, A. Kokalj, M. Lazzeri, L. Martin-Samos, N. Marzari, F. Mauri, R. Mazzarello, S. Paolini, A. Pasquarello, L. Paulatto, C. Sbraccia, S. Scandolo, G. Sciauzero, A. P. Seitsonen, A. Smogunov, P. Umari, and R. M. Wentzcovitch, *Journal of Physics: Condensed Matter* **21**, 395502 (2009).
- ³⁸ P. Giannozzi, O. Andreussi, T. Brumme, O. Bunau, M. B. Nardelli, M. Calandra, R. Car, C. Cavazzoni, D. Ceresoli, M. Cococcioni, N. Colonna, I. Carnimeo, A. D. Corso, S. de Gironcoli, P. Delugas, R. A. DiStasio, A. Ferretti, A. Floris, G. Fratesi, G. Fugallo, R. Gebauer, U. Gerstmann, F. Giustino, T. Gorni, J. Jia, M. Kawamura, H.-Y. Ko, A. Kokalj, E. Küçükbenli, M. Lazzeri, M. Marsili, N. Marzari, F. Mauri, N. L. Nguyen, H.-V. Nguyen, A. O. de-la Roza, L. Paulatto, S. Poncé, D. Rocca, R. Sabatini, B. Santra, M. Schlipf, A. P. Seitsonen, A. Smogunov, I. Timrov, T. Thonhauser, P. Umari, N. Vast, X. Wu, and S. Baroni, *Journal of Physics: Condensed Matter* **29**, 465901 (2017).
- ³⁹ J. P. Perdew, K. Burke, and M. Ernzerhof, *Phys. Rev. Lett.* **77**, 3865 (1996).
- ⁴⁰ M. Cococcioni and S. de Gironcoli, *Phys. Rev. B* **71**, 035105 (2005).
- ⁴¹ I. Timrov, N. Marzari, and M. Cococcioni, *Phys. Rev. B* **98**, 085127 (2018).
- ⁴² K. F. Garrity, J. W. Bennett, K. M. Rabe, and D. Vanderbilt, *Computational Materials Science* **81**, 446 (2014).
- ⁴³ K. Okhotnikov, T. Charpentier, and S. Cadars, *Journal of Cheminformatics* **8**, 17 (2016).
- ⁴⁴ K. Hukushima and K. Nemoto, *Journal of the Physical Society of Japan* **65**, 1604 (1996).
- ⁴⁵ N. Rezaei, M. Alaei, and H. Akbarzadeh, *Computational Materials Science* **202**, 110947 (2022).
- ⁴⁶ J. M. D. Coey, M. Venkatesan, and H. Xu, "Introduction to magnetic oxides," in *Functional Metal Oxides* (John Wiley and Sons, Ltd, 2013) Chap. 1, pp. 1–49.
- ⁴⁷ L. Vaugier, H. Jiang, and S. Biermann, *Phys. Rev. B* **86**, 165105 (2012).
- ⁴⁸ T. Saunders and J. Chalker, *Physical review letters* **98**, 157201 (2007).